NASA TECHNICAL NOTE

NASA TN D-2200

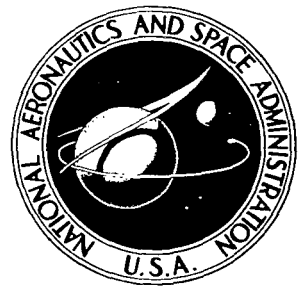




NASA TN D-2200

# BENDING TESTS OF LARGE-DIAMETER STIFFENED CYLINDERS SUSCEPTIBLE TO GENERAL INSTABILITY

*by Michael F. Card*

*Langley Research Center*
*Langley Station, Hampton, Va.*

NATIONAL AERONAUTICS AND SPACE ADMINISTRATION • WASHINGTON, D. C. • APRIL 1964

# BENDING TESTS OF LARGE-DIAMETER STIFFENED CYLINDERS SUSCEPTIBLE TO GENERAL INSTABILITY

By Michael F. Card

Langley Research Center
Langley Station, Hampton, Va.

NATIONAL AERONAUTICS AND SPACE ADMINISTRATION

For sale by the Office of Technical Services, Department of Commerce,
Washington, D.C. 20230 -- Price $0.75

# BENDING TESTS OF LARGE-DIAMETER STIFFENED CYLINDERS SUSCEPTIBLE TO GENERAL INSTABILITY

By Michael F. Card

## SUMMARY

Seven ring-and-stringer stiffened, circular cylinders were loaded to failure in bending. At low loadings, portions of the skin in each of the cylinders buckled locally; the overall load distribution in the cylinders, however, could be predicted analytically up to failure. Failure of all but one of the cylinders is believed to have been precipitated by general instability. Correlation between orthotropic buckling theory and experiment was found to be fairly good, discrepancies being attributed mainly to uncertainties in two of the orthotropic stiffnesses. Efficient weight-strength capabilities of the test cylinder configuration for lightly loaded missile or aircraft applications are indicated.

## INTRODUCTION

Ring-and-stringer stiffened cylinders are often used as aircraft fuselages or missile interstage structures to carry bending and compression loads. Under these loading conditions and depending on the individual geometry, such a structure is prone to one of two major types of instability: panel instability or general instability. Panel instability is usually defined as buckling in a mode in which only the skin and stringers between rings participate in the buckling distortions and thus the rings have no radial deformation. General instability is defined as buckling in a mode in which the rings as well as the skin and stringers are involved in radial buckling distortions. For certain combinations of cylinder geometry, the predicted instability loads for each of the two modes may be nearly identical. Cylinders whose geometry falls in this category are of interest for the design of structures that are efficient from a weight-strength standpoint. Thus, the ability to predict the conditions under which each of these modes will occur is important in the instability analysis of this type of shell structure.

For stiffened cylinders subject to compressive panel instability, reasonable correlation between analytical and experimental results can be found in references 1 and 2. Such correlation is not available for general instability. Although theoretical studies of general instability resulting from either compression or bending loads have appeared at various times in the literature (see, for example, refs. 3 and 4), no comprehensive experimental investigations have been conducted since the work of Hoff and associates from 1943 to 1948 (see,

for example, ref. 5). Correlation between theory and experiment in the latter investigation required certain empirical factors which were based on cylinders of unrealistic proportions in light of present-day aeronautical and aerospace applications. The number and shape of stringer sections as well as the diameter of the test cylinders in the study of reference 5 make extrapolation of the results infeasible for contemporary shell structures.

In order to provide experimental data on general instability in cylinders of more modern proportions, a series of bending tests on seven 77-inch-diameter, circular cylinders, stiffened by both rings and stringers have been conducted at the Langley Research Center structures laboratory. The structural parameters varied were the ring spacing, the stringer spacing, and the ring depth. The cylinder ring sections were purposely made small in order that the structures might be susceptible to a general instability buckling mode.

The general instability data obtained were compared with instability predictions based on orthotropic cylinder theory. The predictions of the orthotropic stiffnesses necessary for the instability calculations were necessarily approximate because the geometry was such that local buckling of the cylinder skin preceded overall instability. In an effort to define these stiffnesses, analytical studies of the load distribution in the cylinders as well as the sensitivity of instability predictions to uncertainties in certain wall stiffnesses were performed. Conservative stiffness values were adopted to compare orthotropic instability theory with experiment.

## SYMBOLS

| | |
|---|---|
| $A_s$ | cross-sectional area of stringers, sq in. |
| $D_x, D_y$ | bending stiffnesses of orthotropic plate in longitudinal and circumferential directions, respectively, in.-kips |
| $D_{xy}$ | twisting stiffness of orthotropic plate, in.-kips |
| $E$ | Young's modulus, ksi |
| $E_x, E_y$ | extensional stiffnesses of orthotropic plate in longitudinal and circumferential directions, respectively, kips/in. |
| $G$ | shearing modulus, ksi |
| $G_{xy}$ | in-plane shear stiffness of orthotropic plate, kips/in. |
| $M$ | applied moment, in.-kips |
| $M_{bu}$ | moment at flat-plate buckling stress, in.-kips |
| $M_{cr}$ | moment at buckling (general or panel instability), in.-kips |

| | |
|---|---|
| $N_x$ | compressive load per inch in longitudinal direction, kips/in. |
| $N_{x_o}$ | allowable compressive load per inch in longitudinal direction, kips/in. |
| R | radius of cylinder to skin midplane, in. |
| a | test-section length, in. |
| b | stringer spacing, in. |
| d | density of material, lb/cu in. |
| h | depth of ring, in. |
| $l$ | ring spacing, in. |
| $l_r$ | ring width, in. (see fig. 1) |
| m,n | number of half-waves into which cylinder buckles in longitudinal and circumferential directions, respectively |
| t | thickness of cylinder skin, in. |
| $\bar{t}$ | cross-sectional area of shell per inch of circumference expressed as an equivalent thickness, in. |
| $\gamma$ | empirical correlation factor for orthotropic cylinders (ref. 11) |
| $\mu_x,\mu_y$ | Poisson's ratios associated with bending of orthotropic plate in longitudinal and circumferential directions, respectively |
| $\mu_x',\mu_y'$ | Poisson's ratio associated with extension of orthotropic plate in longitudinal and circumferential directions, respectively |
| $\sigma$ | stringer stress in cylinder, ksi |
| $\bar{\sigma}$ | maximum stringer stress in cylinder, ksi |
| $\bar{\sigma}_{cr}$ | calculated maximum stringer stress in cylinder at measured $M_{cr}$, ksi |
| $\sigma_{bu}$ | flat-plate buckling stress, ksi |
| $\sigma_e$ | edge stress in infinitely long plate, ksi |
| $\varphi$ | circumferential coordinate, deg |

## TEST SPECIMENS AND TEST PROCEDURES

### Specimens

The test specimens consisted of seven 77-inch-diameter cylinders, stiffened on the outer surface with extruded Z-section stringers and on the inner surface with small, formed hat-section rings. In order to prevent end failures, two sturdy hat-section rings were used to stiffen the ends of each of the specimens. The rings were riveted to the cylinder skin whereas the stringers were spot-welded. The stringer and ring sections in each cylinder were identical except for the ring depth. The dimensions of the small rings and stringers as well as the overall dimensions of the individual cylinders are given in figure 1 and in table I. Average values of the stringer area and skin thicknesses are presented; all other dimensions indicated are nominal. The cylinders have been divided into two groups differentiated by cylinder ring depth $h$ as well as by stringer-spacing—skin-thickness ratio $b/t$. The $b/t$ ratios for groups I and II are 125 and 200, respectively, and are such that local buckling of the cylinder skin occurred very early in the loading history of each test specimen.

The cylinders were constructed of 7075-T6 aluminum alloy. Typical material properties were used in reducing the data: Young's modulus $E$ was assigned the value of 10,500 ksi; the shearing modulus $G$, the value 4,000 ksi; and Poisson's ratio, the value 0.32.

### Procedures

The cylinders were loaded in bending through a loading frame with the use of a hydraulic jack. A photograph of the test setup is shown in figure 2. Effects of stray loads, frictional forces, and weights of fixtures, which are ordinarily present in tests such as these, were minimized insofar as practicable with the use of rollers and counterbalancing weights as described in reference 6. Each cylinder was instrumented with several resistance-type wire strain gages. Two types of gages were used. Gages with a $\frac{13}{16}$-inch-gage length were employed on the cylinder skin to detect local buckling; gages with a 6-inch-gage length mounted on the stringers were used to detect the overall buckling of the cylinder wall and to indicate stress distribution in the cylinder. The 6-inch gages were mounted in back-to-back pairs and distributed circumferentially along two longitudinal stations as indicated in figure 3. The strains from the gages were recorded at a virtually continuous rate either on autographic strain recorders or on the Langley central digital data recording system. For each specimen, both a local buckling test at low loadings and a test to failure were conducted. The skin gages were recorded only during the local buckling test.

## TEST RESULTS

### Local Buckling

In spite of the precautions taken with the test fixtures, the strain gages as well as visual observations indicated that the first skin buckles did not occur at the locations expected. In fact, skin buckling in isolated areas was observed on all of the group II cylinders as the ends of the cylinders were being bolted to the fixtures. However, the strain-gage data indicated that premature skin buckling had little effect on the overall stress distribution in the specimens after a small bending load had been applied. For group I cylinders, buckling of the skin was not observed until a bending moment had been applied. For both groups of cylinders, most of the skin buckling in the areas of high compressive stress occurred at about 75 percent of the load predicted for a curved plate with edge supports equivalent to that of the test cylinders. (See ref. 7.) Since the predicted buckling stress was small (4.2 ksi for group I cylinders, 1.8 ksi for group II cylinders), the presence of small stray loads or built-in fabrication stresses may have accounted for the premature local buckling.

### Failure Tests

The applied moment at which failure occurred is given in table I. In all the tests, overall buckling was accompanied by a catastrophic collapse of the cylinder wall. Observations of the buckling pattern after failure indicated that one or more of the rings were distorted in all except one of the cylinders tested. Table I indicates the mode of buckling of each cylinder based on these observations. Figure 4 shows two of the cylinders after failure. The cylinder shown in figure 4(a) is believed to have buckled in the general instability mode and is typical of most of the cylinders. Figure 4(b) indicates the mode of failure of the only cylinder believed to have buckled in the panel instability mode.

### Loading History

The loading histories of the cylinders are indicated in figures 5 and 6. In figure 5, stresses at various locations in the compressive areas of each cylinder have been plotted against the circumferential coordinate $\varphi$. Values are shown for two bending moments: $M_{cr}$ the moment at failure, and $\frac{1}{2}M_{cr}$. The circles and squares represent data obtained from the measured values of strain at two longitudinal stations A and B on the cylinder. (See fig. 3.) The values shown are the average of back-to-back gages on the stringer web. Individual gages had a maximum deviation of $\pm 2$ percent from the average value employed in constructing the figure.

The curves shown in figure 5 have been calculated by an iterative procedure. Because some areas of the cylinder skin were buckled under the applied bending moment, the stress distribution in the cylinder skin was no longer

linear. Approximate techniques to describe the load carried by the buckled skin were employed. Each cylinder was divided into elements defined by a stringer and a width of skin equal to the stringer spacing. A strain and the corresponding stress $\overline{\sigma}$ were specified in the extreme compressive element; a distribution of stringer stresses varying linearly with depth was assumed; and the corresponding axial load on each element was computed. The effective width formula of reference 2 was employed for the estimation of the load carried by those elements with buckled skin. The local buckling stress required by the formula of reference 2 was obtained from reference 7 for a flat plate of geometry similar to the cylinder skin panels and elastically restrained by stringers. By using these approximations, the net axial load on the cylinder was computed. Iteration with various linear stress distributions was performed until the axial load on the cylinder was negligibly small. With the stress distribution necessary for axial-force equilibrium, the applied moment corresponding to the specified stress was computed by numerical integration of the loads in the cylinder elements.

It can be seen from figure 5 that the agreement between experiment and calculation is reasonably good for most of the cylinders except for cylinder 4, group II. (See fig. 5(g).) Although agreement for this cylinder is only fair at lower values of applied moment M, it seems to improve somewhat with increased loading. The curve for $M = \frac{3}{4}M_{cr}$ has been included in figure 5(g) to indicate this trend.

In figure 6, the applied moment has been plotted against the maximum compressive stress in the cylinder. The circles are the average of the data obtained from the most highly compressed stringer in each cylinder. As indicated in figure 5, this stringer was located at or very near the geometric extreme compressive fiber. From figures 5 and 6, it can be seen that all measured strains in the stringers corresponded to elastic stresses in the material.

The curves of figure 6 were obtained from the previously mentioned iterative procedure. The lower tick marks on each of the curves indicate the moment $M_{bu}$ corresponding to the stress computed for buckling of flat skin panels of the cylinder geometry. The upper tick mark indicates the maximum moment $M_{cr}$ that the cylinder carried before collapse. The ratio of stresses corresponding to these moments is given in table I. It can be seen from both figures 5 and 6 that the overall loading history of the cylinders was predicted analytically with reasonable accuracy in spite of the somewhat random and premature skin buckling mentioned earlier.

## INSTABILITY ANALYSIS

A common approach to the buckling analysis of ring-and-stringer stiffened shells is to consider the shell wall as an orthotropic material. To form the mechanical properties of orthotropic shells in which the stiffening members are rather closely spaced, the discrete stiffnesses of individual elements can be analytically "smeared" into effective wall stiffnesses. The latter are then inserted into an orthotropic shell buckling equation in order to predict the

instability loads. For the case of the ring-and-stringer stiffened cylinder in which the skin is severely buckled, the wall stiffnesses are not only functions of geometry but are also functions of the state of stress of the cylinder skin. These stiffnesses are difficult to estimate analytically and, therefore, the possible range of their magnitudes and their effect on the buckling load deserves consideration.

## General Instability

To predict general instability loads for the test cylinders, the orthotropic compressive stability equation of reference 4 was adopted. The equation employed was

$$N_x = \left(\frac{m\pi}{a}\right)^2\left[\frac{D_x}{1-\mu_x\mu_y} + \left(\frac{\mu_y D_x}{1-\mu_x\mu_y} + 2D_{xy} + \frac{\mu_x D_y}{1-\mu_x\mu_y}\right)\left(\frac{n}{m}\right)^2\left(\frac{a}{2\pi R}\right)^2 + \frac{D_y}{1-\mu_x\mu_y}\left(\frac{n}{m}\right)^4\left(\frac{a}{2\pi R}\right)^4\right]$$

$$+ \frac{E_x E_y}{\left(\frac{m\pi}{a}\right)^2 R^2\left[E_x - \left(\mu_y' E_x - \frac{E_x E_y}{G_{xy}} + \mu_x' E_y\right)\left(\frac{n}{m}\right)^2\left(\frac{a}{2\pi R}\right)^2 + E_y\left(\frac{n}{m}\right)^4\left(\frac{a}{2\pi R}\right)^4\right]} \qquad (1)$$

where the transverse shear stiffness considered in the stability equation of reference 4 has been assumed to be infinitely large. Equation (1) is valid for simply supported cylinders. It is also assumed to be valid for cylinders with other edge support which are moderately long, that is, long enough so that the axial buckle wave length is not influenced by boundary conditions. The reciprocal relations of reference 4

$$\left.\begin{aligned} \mu_x D_y &= \mu_y D_x \\ \mu_x' E_y &= \mu_y' E_x \end{aligned}\right\} \qquad (2)$$

were employed so that equation (1) is a function of eight stiffnesses.

The buckling solution of equation (1) requires minimization of the compressive load per inch $N_x$ with respect to integral values of $m$ and $n$, the number of half-waves of the buckle pattern in the longitudinal and circumferential directions, respectively. In addition, for those stiffnesses which are functions of the state of stress of the buckled cylinder skin, compatibility between the buckling stress and the stiffness assumed in finding that stress must be satisfied. To fulfill these requirements, the general instability computations presented in this report were performed by an iteration procedure on a digital computer. In the computations, the analytical loading history curves of figure 6 were employed to convert the buckling load per inch $N_x$ to an applied moment.

For instability modes obtained from equation (1) to be considered as general instability modes, the axial half wave length obtained after minimization should include at least one or more rings. (See fig. 14 of ref. 3.) The computations made for the cylinders indicated that this condition was fulfilled in every case. Also, the axial half wave length must be small compared with the length a in equation (1). It was necessary to define the length a in terms of the geometry of the cylinders. The length was taken as that measured between two sturdy hat-section rings stiffening the ends of the cylinder test section and is indicated in figure 4(a). By using this length for all computations, it was found that the minimum buckling load obtained was insensitive to variations in the number of longitudinal half-waves m, so that the cylinders, for analytical purposes, could be considered as moderately long. Thus equation (1) would appear to be valid as a criterion for general instability of the test cylinders.

## Stiffnesses for Base Calculation

The difficulties of estimating the stiffnesses appearing in equation (1) for stiffened cylinders with buckled skin have already been mentioned. Certain stiffnesses such as the longitudinal bending and extensional stiffnesses $D_x$ and $E_x$ appear to be reasonably well defined. The correlation achieved between calculation and experiment in predicting the loading histories of the test cylinders (figs. 5 and 6) indicate that $E_x$ for the test cylinder configuration can be predicted accurately. The fact that $D_x$ can be derived from the same effective width formula used in determining $E_x$ suggests that it also can be estimated with reasonable accuracy. The other stiffnesses in equation (1) are less well defined and only approximate predictions of these stiffnesses can be made at best.

To predict general instability for the test cylinders of this report, a base calculation, in which generally conservative values of orthotropic stiffnesses were defined, was adopted for use in equation (1). The values of stiffnesses used in the calculation were as follows:

(a) Poisson's ratios $\mu_x$, $\mu_x'$, $\mu_y$, and $\mu_y'$ were set equal to zero.

(b) The longitudinal extensional and bending stiffnesses $E_x$ and $D_x$ were taken from reference 2 as

$$E_x = E\left(\frac{A_s}{b} + \frac{\bar{E}_{sec}}{E}\, t\right)$$

and

$$D_x = \frac{EI_s}{b}\left[1 + \frac{(y_s/\rho_s)^2}{1 + \dfrac{A_s}{\dfrac{\bar{E}_{tan}}{E}\, bt}}\right]$$

where $A_s$ is the area of the stringer section; $I_s$ is the moment of inertia of the stringer section about its center of gravity; $y_s$, the distance between the center of gravity of the stringer and the middle plane of the cylinder skin; and $\rho_s$, the radius of gyration of the stringer. $\overline{E}_{sec}$ and $\overline{E}_{tan}$ are the secant and tangent moduli of the buckled skin, respectively, and can be obtained from equations (A2) and (A3) of reference 2. The reference equations are based on the effective width formula used in predicting the loading histories for the test cylinders.

(c) The twisting stiffness $D_{xy}$ was computed with the expression

$$D_{xy} = \frac{1}{2}\left(\frac{GJ_s}{b} + \frac{GJ_r}{l} + \frac{Gt^3}{3}\right)$$

where $GJ_s$ is the twisting stiffness of the stringer section and $GJ_r$ is the twisting stiffness of the closed section formed by the ring and skin between ring rivets.

(d) The circumferential extensional stiffness $E_y$ was obtained by considering the contribution to the stiffness by the buckled skin to be equal to that for $E_x$, that is,

$$E_y = E\left(\frac{A_r}{l} + \frac{\overline{E}_{sec}}{E}\, t\right)$$

where $A_r$ is the cross-sectional area of the ring.

(e) The circumferential bending stiffness $D_y$ was taken to be the value computed for the ring and a portion of skin equal to the ring width $l_r$ (see fig. 1(b)) by employing the expression

$$D_y = \frac{EI_r}{l}\left[1 + \frac{(y_r/\rho_r)^2}{1 + \frac{A_r}{l_r t}}\right]$$

where $I_r$ is the moment of inertia of the ring section about its center of gravity; $y_r$, the distance between the center of gravity of the ring and the middle plane of the cylinder skin; and $\rho_r$, the radius of gyration of the ring.

(f) For the shearing stiffness $G_{xy}$, the value given in reference 8 for a flat strip was adopted. In figure 7, the effective shear stiffness taken from the reference has been plotted against the edge stress ratio $\sigma_e/\sigma_{bu}$.

To compute the base general instability loads, the stiffnesses defined by the base calculation were inserted into equation (1) and the appropriate minimization performed.

## Comparison of Analysis With Experiment

In figure 8, a comparison of calculated results is made with the cylinder test data. The circles on the figure represent the bending moment at failure for the two groups of cylinders. The general instability curves shown are the result of employing equation (1) with the stiffnesses defined in the base calculation mentioned previously. The calculations are about 10 percent conservative for the group I cylinders and 20 to 30 percent conservative for group II. The experimental trends are predicted reasonably well.

Figure 8 gives no indication of the effects of the particular choice of stiffness parameters in the base calculation. A study of the sensitivity of the general instability predictions to the choice of certain stiffness parameters was undertaken, however, and is presented in the appendix. The essential results of this study were that the general instability curves shown in figure 8 could be affected considerably by the magnitudes of the circumferential bending stiffness $D_y$ as well as the shearing stiffness $G_{xy}$. In the base calculation, these stiffnesses are estimated conservatively; hence, the curves shown in figure 8 might be expected to lie below the data.

The susceptibility of the test cylinders to panel instability is also indicated in figure 8. The panel instability curve shown was computed by equation (3) of reference 2. With respect to panel instability, all of the test cylinders fall into the so-called "short" cylinder range so that some estimate of the end fixity provided by the cylinder rings is required. The curve shown in the figure was computed for the group II cylinders with an assumed value of 2.0 for the column fixity coefficient of equation (3). The value was chosen so the curve shown would approximate the experimental buckling load obtained for cylinder 4, group II. In addition to being the longest cylinder tested (and hence the most susceptible to panel instability), this cylinder was the only one in which the rings appeared to have no radial deformation. (See fig. 4(b).) The curve indicates that the other cylinders in the group, by virtue of their shorter lengths, should have buckled in the general mode rather than in the panel instability mode. Thus only one cylinder of this group seems susceptible to panel instability. For group I, the use of even the minimum column fixity coefficient (1.0) in equation (3) gives loads much higher than that required for general instability so that none of the cylinders in this group are susceptible to panel instability.

# DISCUSSION

## General Instability Predictions

It is evident that the preciseness of general instability predictions for the test cylinders of this report is hampered by the approximate nature of the

stiffnesses that were inserted in the stability equation. The stiffness study contained in the appendix indicates that the lack of agreement between orthotropic theory and experiment of figure 8 is probably not associated with the use of uncertain values for the stiffnesses $\mu_x$, $\mu_x'$, $D_x$, $E_x$, $D_{xy}$, and $E_y$. These stiffnesses are either reasonably well defined analytically, as in the case of $E_x$ and $D_x$, or else their uncertainties have little effect on the magnitude of the general instability load. Hence, the stiffnesses $D_y$ and $G_{xy}$ remain as a probable cause of the discrepancy between theory and experiment.

It should be noted that the group I cylinders buckled at a stress ratio $\bar{\sigma}_{cr}/\sigma_{bu}$ of about half that of the group II cylinders. (See table I.) Therefore, if $D_y$ and $G_{xy}$ are indeed the cause of the discrepancy, the values of these stiffnesses would have to be increased more for highly buckled skin than for moderately buckled skin to bring predictions and experiment into agreement. The possibility of these effects has been suggested (refs. 9 and 10) but it is apparent that more substantiated, quantitative studies of these stiffnesses are needed.

A further cause of discrepancy between theory and experiment might be attributed to the customary lack of agreement between small-deflection buckling theory and experiment. A correlation factor is usually applied to buckling computations to bring them into better agreement with experiment. For orthotropic cylinders there is a lack of experimental information upon which to base this empirical parameter. Reference 11, however, has suggested a correlation factor $\gamma$ which has been applied to a limited amount of orthotropic cylinder data. This factor, if applied to the present tests indicates that the group II base calculation would be changed by at most 4 percent (cylinder 4); the group I calculation would be essentially unaffected. It appears, then, that on the basis of the limited cylinder data available, reasonable correlation between orthotropic small-deflection buckling theory and experiment would be expected for the test cylinders provided the cylinder wall stiffnesses were known accurately. The lack of agreement between the test data and the buckling computations obtained herein probably does not stem from the use of small deflection buckling theory but rather from the uncertainties in individual orthotropic stiffnesses.

Another effect, which has not been considered in the theoretical calculations for general instability presented is that of the asymmetry (one-sided stiffening) of the walls of the test cylinders. In references 3, 12, and 13, studies of asymmetric effects on general instability predictions have been made for orthotropic shells loaded by compression or external pressure. There is some indication in these references that, for stiffened cylinders with small ratios of radius to thickness, asymmetry can have a substantial effect on instability predictions. Attempts to use the results of reference 3 to predict general instability for the test cylinders, however, indicate that asymmetric effects are negligible for the cylinders because of their large radii.

## Weight-Strength Considerations

The test cylinder design is somewhat unusual in that, unlike conventional aeronautical designs, the cylinder walls are stiffened by extremely light rings. It seems desirable, therefore, to determine the relative structural efficiency of the cylinder configuration. In figure 9, a comparison is made between the relative efficiencies for four types of cylinder construction and the test cylinders. The curves shown on the figure were obtained from figure 14 of reference 11. The circles and squares shown correspond to the data obtained from the cylinders of this report. The parameter $N_{x_o}/R$ has been calculated by converting the maximum cylinder stresses obtained from the curves of figure 6 to a load per inch of circumference by employing the effective width formula of reference 2. The weights of the cylinder test section including the stiffening rings were incorporated into the parameter $d\bar{t}/R$.

Since weight optimization was not a primary consideration in designing the test cylinders, the data shown in figure 9 indicate only the approximate position of the ring-and-stringer stiffened cylinder with buckled skin in comparison with other types of stiffening. The figure indicates that this type of construction is more efficient for the loading index range 0.01 to 0.03 ksi than either the waffle-like construction or longitudinally stiffened construction having unbuckled skin. For long cylindrical structures, intermediate rings (not included in the weight-strength analysis of ref. 11) are usually added to meet loading conditions other than compression. For the ring-and-stringer stiffened cylinder, these rings are an inherent part of the stiffening; hence, the weight comparison between it and the other types of cylinder construction (including the sandwich type) should be even more favorable for the ring-and-stringer stiffened cylinder than that shown on the figure.

## CONCLUDING REMARKS

Results of bending tests on seven, large-diameter, stiffened cylinders have been presented and discussed. Although the cylinder skin buckled in areas of high compression during the tests, the load distribution in each of the test cylinders was predicted analytically with reasonable accuracy up to overall instability. An attempt was made to analyze the overall instability behavior by using orthotropic theory from the standpoint of both general and panel instability. On the basis of visual observation and analysis all but one of the test cylinders are believed to have failed in the general instability mode. The general instability analysis is in fairly good agreement with the data. The discrepancies between analysis and experiment are attributed to a lack of precise knowledge of magnitudes of the orthotropic stiffnesses $D_y$ and $G_{xy}$. Weight-strength considerations of the cylinders suggest that ring-and-stringer stiffened shells in which the cylinder skin is permitted to buckle is a rather efficient design for lightly loaded structures.

Langley Research Center,
National Aeronautics and Space Administration,
Langley Station, Hampton, Va., December 10, 1963.

## APPENDIX

## SENSITIVITY OF GENERAL INSTABILITY PREDICTIONS TO ORTHOTROPIC STIFFNESSES

Because the magnitudes of certain stiffnesses were computed by very approximate formulas, the base calculation employed for general instability predictions has a certain arbitrariness in its definition. It would seem appropriate, therefore, to investigate the individual stiffnesses in the stability equation to estimate the effects of uncertainties in stiffness magnitudes on the instability predictions.

In the following section, each of the stiffnesses appearing in equation (1) is discussed and, where possible, an attempt is made to justify the expressions employed for the particular stiffness in the base calculation. For estimating the magnitudes of certain stiffnesses in equation (1), however, there are no substantiated analytical techniques available. To study the effects of uncertainties in these stiffnesses, additional instability calculations using equation (1) were performed for the test cylinders. Instability predictions were made with the method of computing the specific stiffness in question varied from that employed in the base calculation. The differences in computed instability loads between these calculations and those of the base calculation were then used as a criterion to determine the sensitivity of general instability predictions to uncertainties in magnitude of the stiffnesses considered.

### Orthotropic Stiffnesses

$\mu_x$, $\mu_x'$, $\mu_y$, and $\mu_y'$.- To determine the appropriate value of $\mu_x$ and $\mu_x'$ for a cylinder with severely buckled skin, it is necessary to investigate the postbuckling behavior of curved plates loaded in compression. Reference 2 has suggested that the behavior of curved panels in cylinders may be approximated by flat-plate postbuckling theory in the advanced stages of postbuckling. Figure 10 indicates results for $\mu_x'$ taken from the flat-plate study of reference 9. At large values of the edge stress ratio $\sigma_e/\sigma_{bu}$, $\mu_x'$ appears to be small compared with unity. A similar result can be obtained from reference 14. These studies suggest that $\mu_x'$ and $\mu_x$ can probably be taken as zero without introducing large errors in the stability equation; $\mu_y'$ and $\mu_y$ then are also zero from equation (2). Thus, the use of zero for $\mu_x'$ and $\mu_x$ in the base calculation would seem to be reasonable.

$D_x$ and $E_x$.- The results of reference 2 indicate that an adequate knowledge of these stiffnesses exists for the longitudinally stiffened cylinders with buckled skin considered therein. The application of the effective width formula of the reference to the present tests of ring-and-stringer stiffened cylinders gives reasonable correlation between calculation and experiment for

the loading histories of the test cylinders. (See figs. 5 and 6.) This result implies that both $D_x$ and $E_x$ are known with sufficient accuracy for the test cylinders.

$D_{xy}$.- There are no analytical procedures available for obtaining the twisting stiffness $D_{xy}$ for longitudinally and circumferentially stiffened cylinders with buckled sheet. However, when $D_{xy}$ was taken to be zero, the calculated moment at buckling for the test cylinders was found to decrease only from 5 to 10 percent from that of the base calculation. This fact suggests that for the test cylinders, uncertainties in this stiffness had little effect on correlation between orthotropic analysis and experiment.

$E_y$ and $D_y$.- Little analytical information is available for predicting either of these stiffnesses. To consider the effect of uncertainties in $E_y$ alone, a computation was made in which the contribution of the buckled skin was neglected. Because no appreciable change in the predicted buckling load was observed, general instability buckling predictions seem insensitive to uncertainties in $E_y$ alone.

In order to estimate $E_y$ and $D_y$ for cylinders with buckled skin panels, a knowledge of the circumferential stiffness of a buckled, cylindrical plate is required. Reference 14 attempts to predict the transverse stiffness of buckled flat plates and represents the only available source for estimating this stiffness. To apply the results of the reference to estimations of $E_y$ and $D_y$ for the test cylinders, the secant and tangent moduli concept (based on flat-plate behavior) that was used in determining skin contributions for $E_x$ and $D_x$ (ref. 2) was adopted. Because the appropriate loading to obtain the transverse moduli is infinitesimally small, the secant and tangent moduli were both taken as equivalent to the value given in reference 14 for extensional stiffness in the transverse direction of the buckled plate. Formulas similar to those used in the base calculation for the longitudinal extensional and bending stiffnesses were then used to compute $E_y$ and $D_y$. The difference between the dashed and solid curves of figure 11(a) indicates the effect of applying the results of reference 14 in computing $E_y$ and $D_y$. It can be seen that for both group I and group II cylinders, a maximum increase of about 10 percent over the base calculation buckling load was obtained.

In contrast to this consideration, the suggestion has been made in reference 10 that a corrugation effect of the buckled skin panels may even increase their contribution to $D_y$ above the unbuckled skin contribution. The dash-dot curve of figure 11(a) indicates the effect of a variation from the base calculation in which $D_y$ was computed by considering the skin as unbuckled. The effect can be seen to be about the same as that obtained by employing reference 14. This calculation is not intended to set limits on $D_y$ but merely to illustrate the sensitivity of buckling to changes in $D_y$. The calculation suggests that wide variations in $D_y$ could influence the accuracy of buckling computations on cylinders of the proportions considered in this report.

$G_{xy}$.- The effective shear stiffness of buckled sheet has long been recognized as an important structural parameter in predicting general instability. (See ref. 5.) Unfortunately, theoretical studies of this problem have resulted in variations in the proposed stiffness of as much as 100 percent. In fact, there is disagreement as to the trend in magnitude of the stiffness as the load in the buckled plate is increased. (Compare, for example, the results of references 8 and 9.)

Figure 11(b) indicates the effect of variations in $G_{xy}$ on the instability load. The dash-dot curve shows the effect of increasing the base calculation shearing stiffness by 100 percent. The dashed curve on the figure indicates the effect of employing reference 9 in computing the shearing stiffness. The computations show that, because of the analytic discrepancies in the proposed stiffness, buckling predictions can be very sensitive to the choice of this parameter. As in the case of the circumferential stiffnesses, no defined limits can be established on the shearing stiffness until suitable experimental evidence of the true stiffness behavior is obtained.

## REFERENCES


1. Peterson, James P., and Dow, Marvin B.: Compression Tests on Circular Cylinders Stiffened Longitudinally by Closely Spaced Z-Section Stringers. NASA MEMO 2-12-59L, 1959.

2. Peterson, James P., Whitley, Ralph O., and Deaton, Jerry W.: Structural Behavior and Compressive Strength of Circular Cylinders With Longitudinal Stiffening. NASA TN D-1251, 1962.

3. Van der Neut, A.: The General Instability of Stiffened Cylindrical Shells Under Axial Compression. Rep. S. 314, Nat. Aero. Res. Inst. (Amsterdam), 1947.

4. Stein, Manuel, and Mayers, J.: Compressive Buckling of Simply Supported Curved Plates and Cylinders of Sandwich Construction. NACA TN 2601, 1952.

5. Hoff, N. J., Boley, Bruno A., and Nardo, S. V.: The Inward Bulge Type Buckling of Monocoque Cylinders. IV - Experimental Investigation of Cylinders Subjected to Pure Bending. NACA TN 1499, 1948.

6. Peterson, James P.: Bending Tests of Ring-Stiffened Circular Cylinders. NACA TN 3735, 1956.

7. Peterson, James P., and Whitley, Ralph O.: Local Buckling of Longitudinally Stiffened Curved Plates. NASA TN D-750, 1961.

8. Kromm, A., and Marguerre, K.: Behavior of a Plate Strip Under Shear and Compressive Stresses Beyond the Buckling Limit. NACA TM 870, 1938.

9. Stein, Manuel: Behavior of Buckled Rectangular Plates. Jour. Eng. Mech. Div., Proc. American Soc. Civil Eng., vol. 86, no. EM 2, Apr. 1960, pp. 59-76.

10. Argyris, J. H., and Dunne, P. C.: Part 2. Structural Analysis. Structural Principles and Data, Handbook of Aeronautics, No. 1, Pitman Pub. Corp. (New York), 1952, p. 165.

11. Peterson, James P.: Weight-Strength Studies of Structures Representative of Fuselage Construction. NACA TN 4114, 1957.

12. Anon.: Collected Papers on Instability of Shell Structures - 1962. NASA TN D-1510, 1962:

    (a) Hedgepeth, John M.: Design of Stiffened Cylinders in Compression, pp. 77-84.

    (b) Singer, Josef: Buckling of Orthotropic and Stiffened Conical Shells, pp. 463-479.

13. Baruch, M., and Singer, J.: Effect of Eccentricity of Stiffeners on the General Instability of Stiffened Cylindrical Shells Under Hydrostatic Pressure. Jour. Mech. Eng. Sci., vol. 5, no. 1, 1963, pp. 23-27.

14. Van der Neut, A.: The Post-Buckling Stiffness of Rectangular Simply Supported Plates. Rep. VTH-113, Technische Hogeschool Delft Vliegtuigbouwkunde (Delft, Netherlands), Oct. 1962.

TABLE I.- DIMENSIONS AND TEST RESULTS OF CYLINDERS

[Cylinder: radius to skin midplane, R, 38.6 in.; test-section length, a, 72 in.]

| Group | Cylinder | $l$, in. | b, in. | h, in. | t, in. | $A_s$, $in.^2$ | $M_{cr}$, in.-kips | Type of instability | $\frac{\bar{\sigma}_{cr}}{\sigma_{bu}}$ (*) |
|---|---|---|---|---|---|---|---|---|---|
| I | 1 | 6 | 2.48 | 0.54 | 0.0199 | 0.0380 | $5.32 \times 10^3$ | General | 10.8 |
| | 2 | 9 | 2.48 | .54 | .0199 | .0379 | 4.68 | General | 9.4 |
| | 3 | 12 | 2.48 | .54 | .0197 | .0381 | 4.44 | General | 8.8 |
| II | 1 | 6 | 4.04 | 0.30 | 0.0197 | 0.0396 | $3.40 \times 10^3$ | General | 26.3 |
| | 2 | 9 | 4.04 | .30 | .0197 | .0381 | 3.05 | General | 23.2 |
| | 3 | 12 | 4.04 | .30 | .0196 | .0389 | 2.88 | General | 21.6 |
| | 4 | 18 | 4.04 | .30 | .0196 | .0384 | 2.11 | Panel | 15.3 |

*$\bar{\sigma}_{cr}$ corresponds to value read from analytical curves of figure 6.

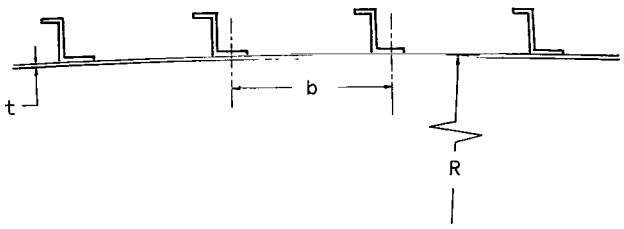


(a) Cylinder wall.

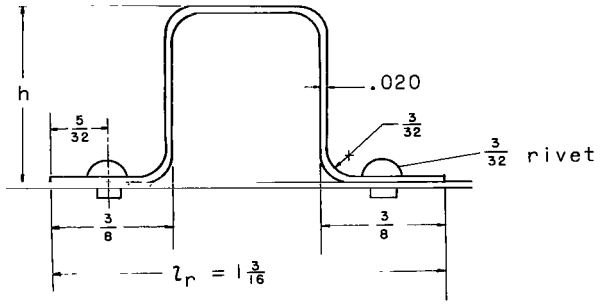


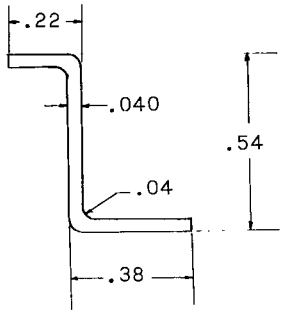


(b) Ring detail.

(c) Stringer detail.

Figure 1.- Dimensions of stiffening elements of test cylinders.

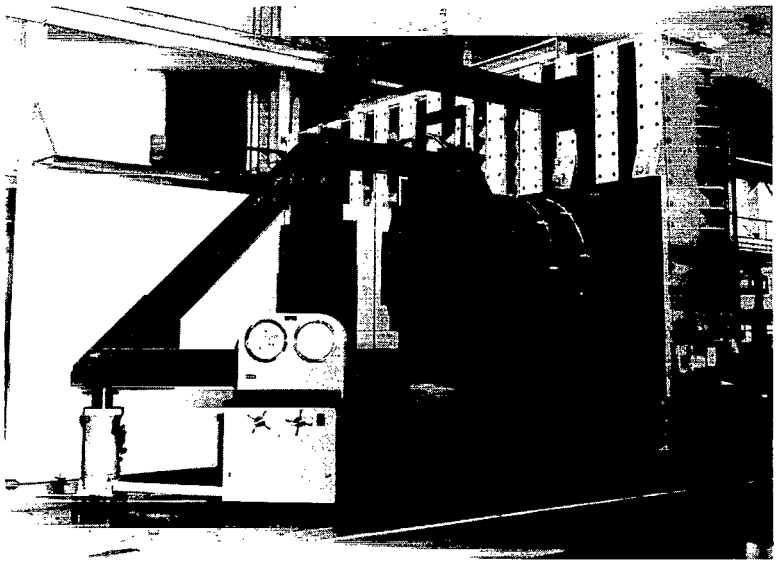

L-60-6548

Figure 2.- General view of test setup showing a 77-inch-diameter cylinder to be tested in bending.

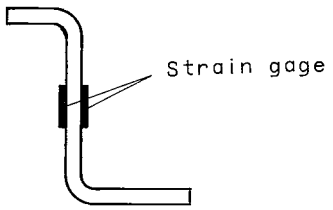


Typical gage position

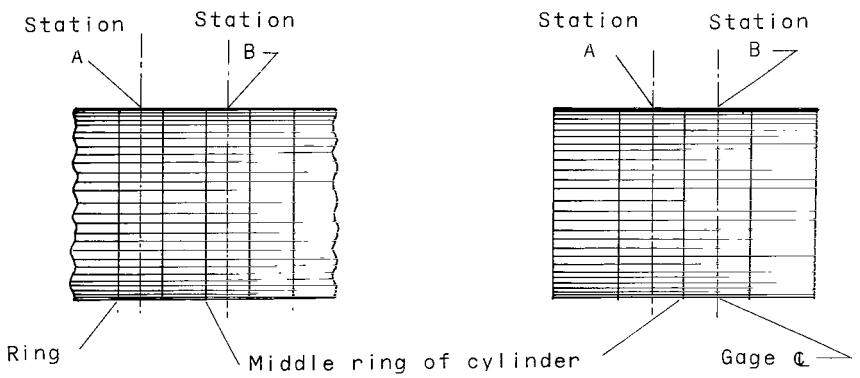


(a) All cylinders excluding cylinder 4, group II.

(b) Cylinder 4, group II.

Figure 3.- Locations of 6-inch strain gages.

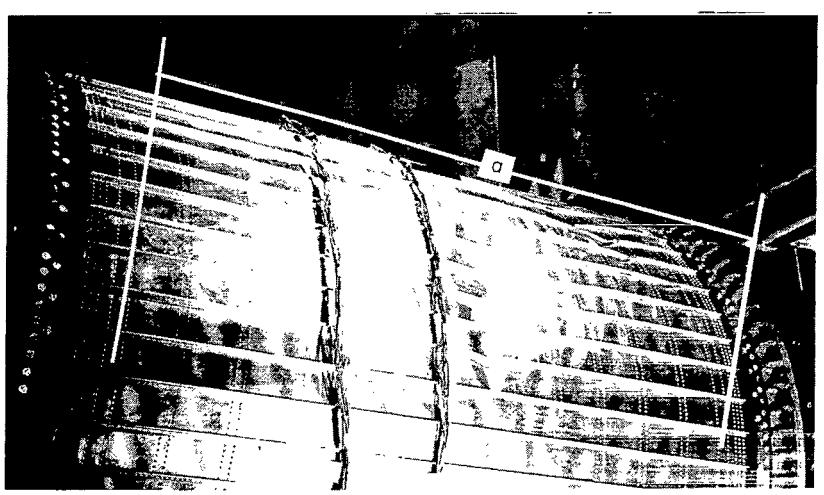


(a) Cylinder 1; group I; general instability.

Figure 4.- Failure of test cylinders.

L-61-1356

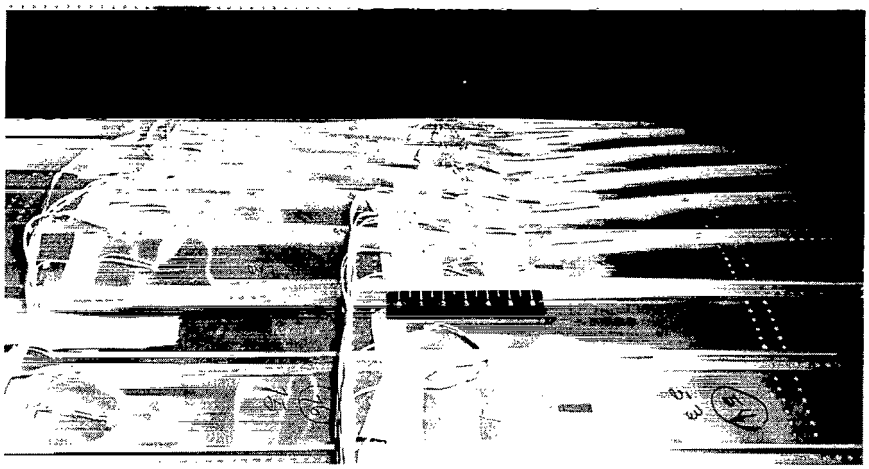

(b) Cylinder 4; group II; panel instability.

Figure 4.- Concluded. L-61-7393

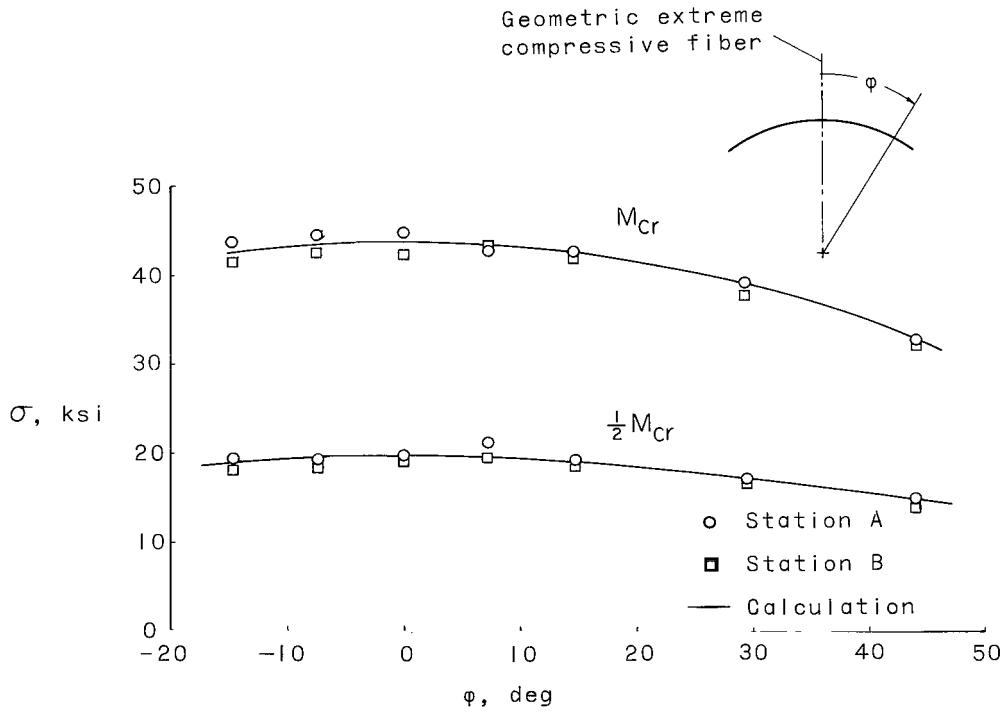


(a) Cylinder 1; group I.

Figure 5.- Stringer stress distribution in test cylinders.

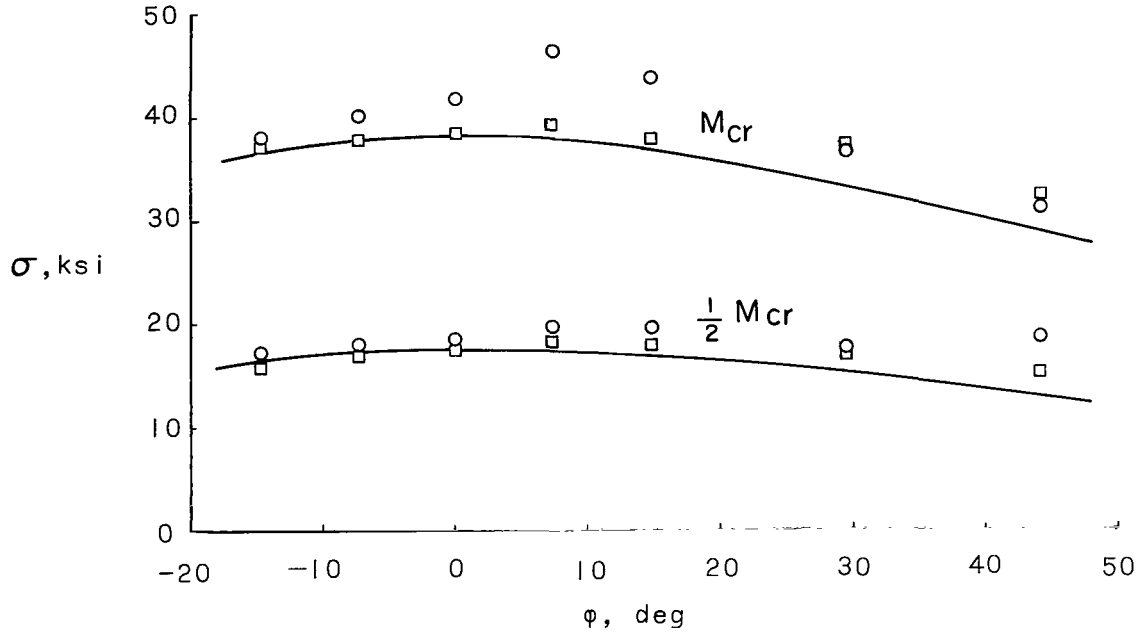


(b) Cylinder 2; group I.

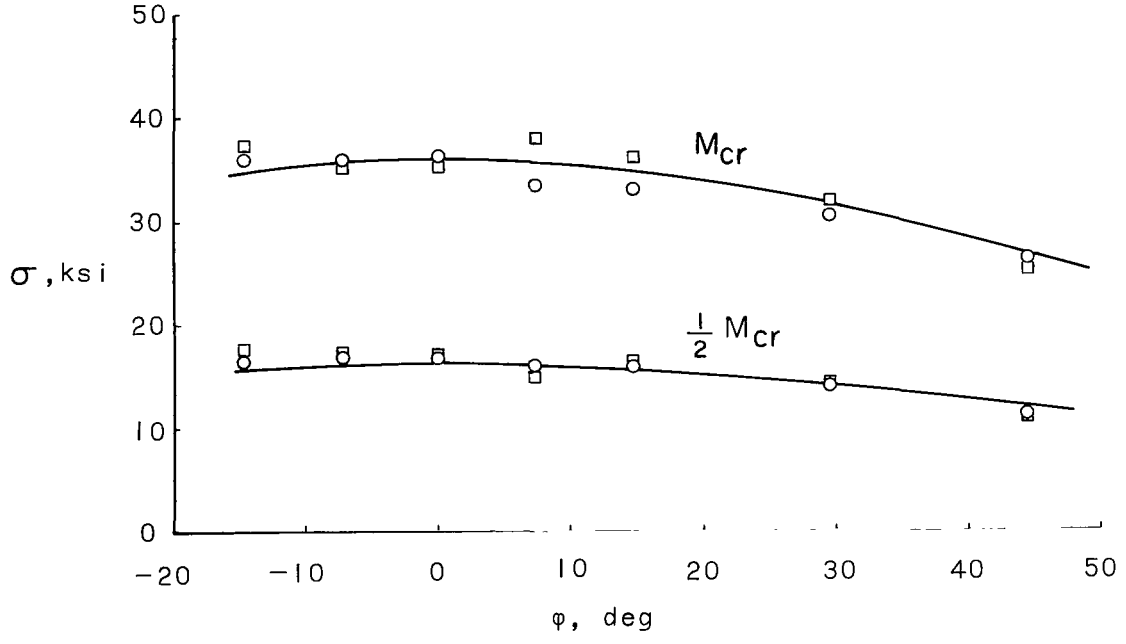


(c) Cylinder 3; group I.

Figure 5.- Continued.

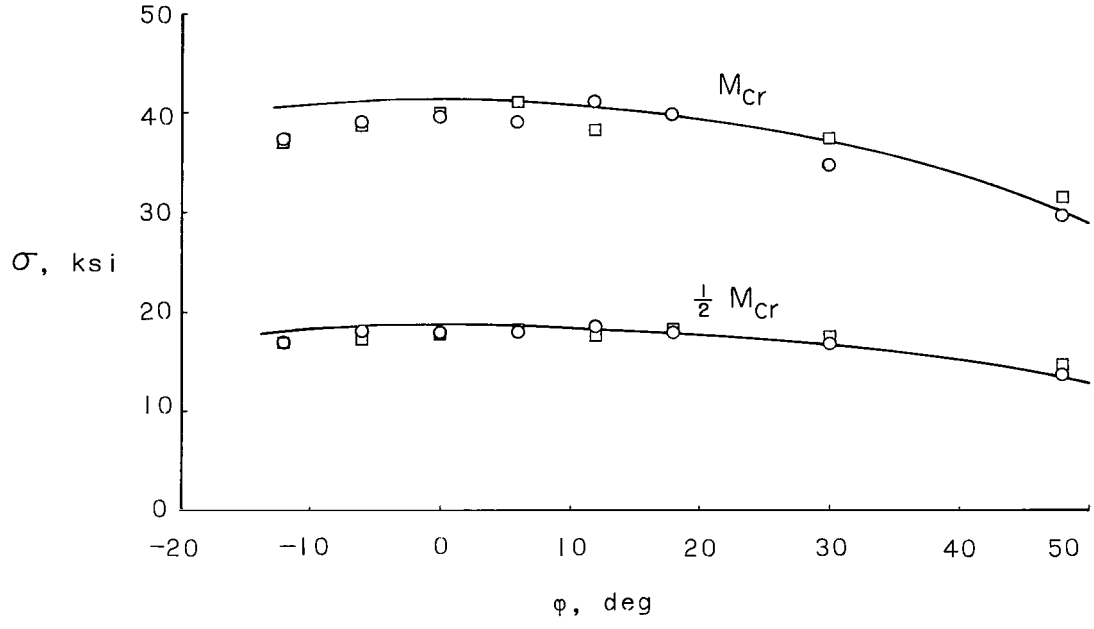


(d) Cylinder 1; group II.

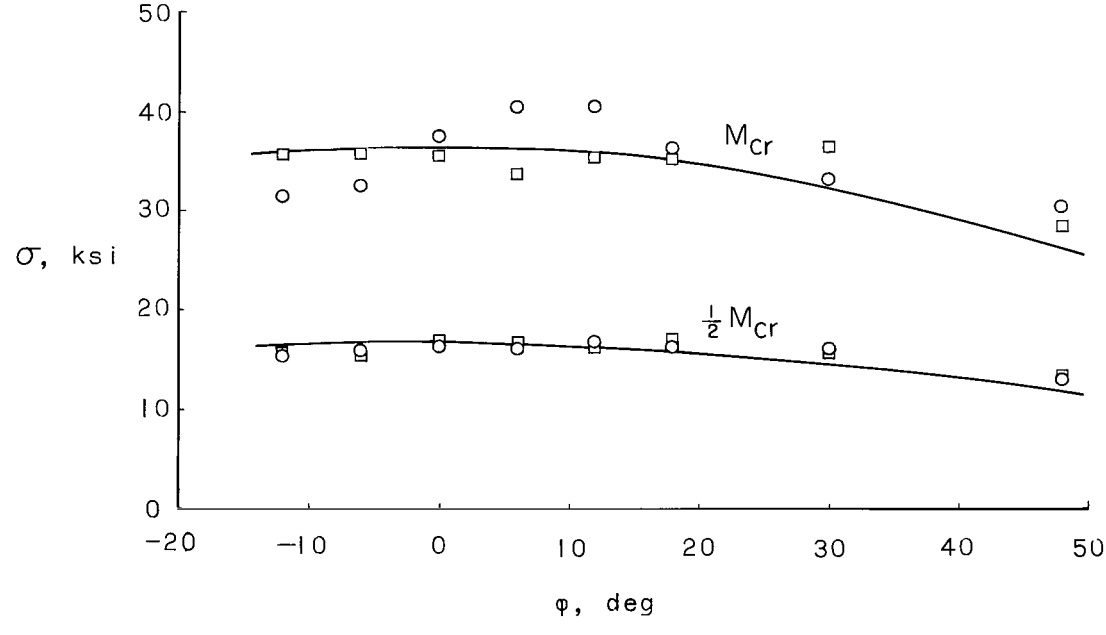


(e) Cylinder 2; group II.

Figure 5.- Continued.

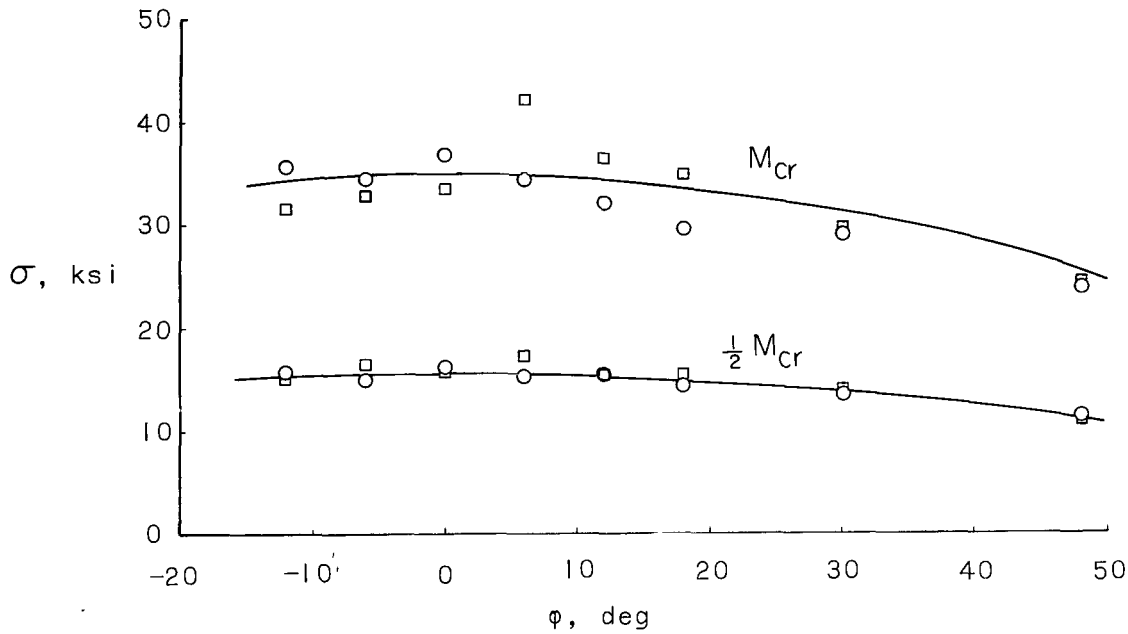


(f) Cylinder 3; group II.

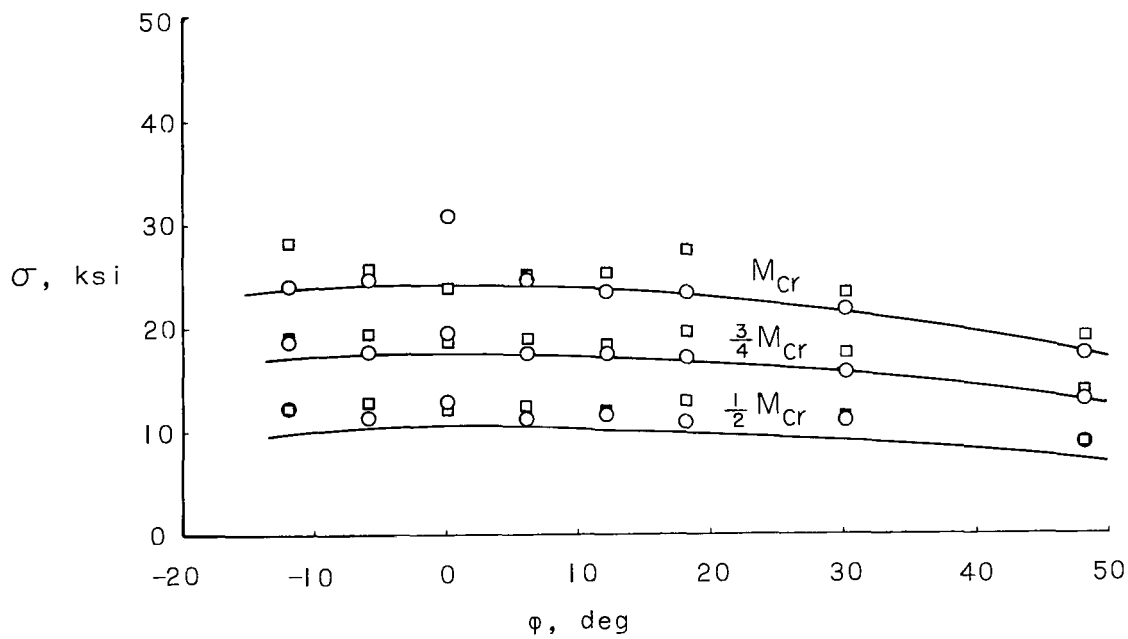


(g) Cylinder 4; group II.

Figure 5.- Concluded.

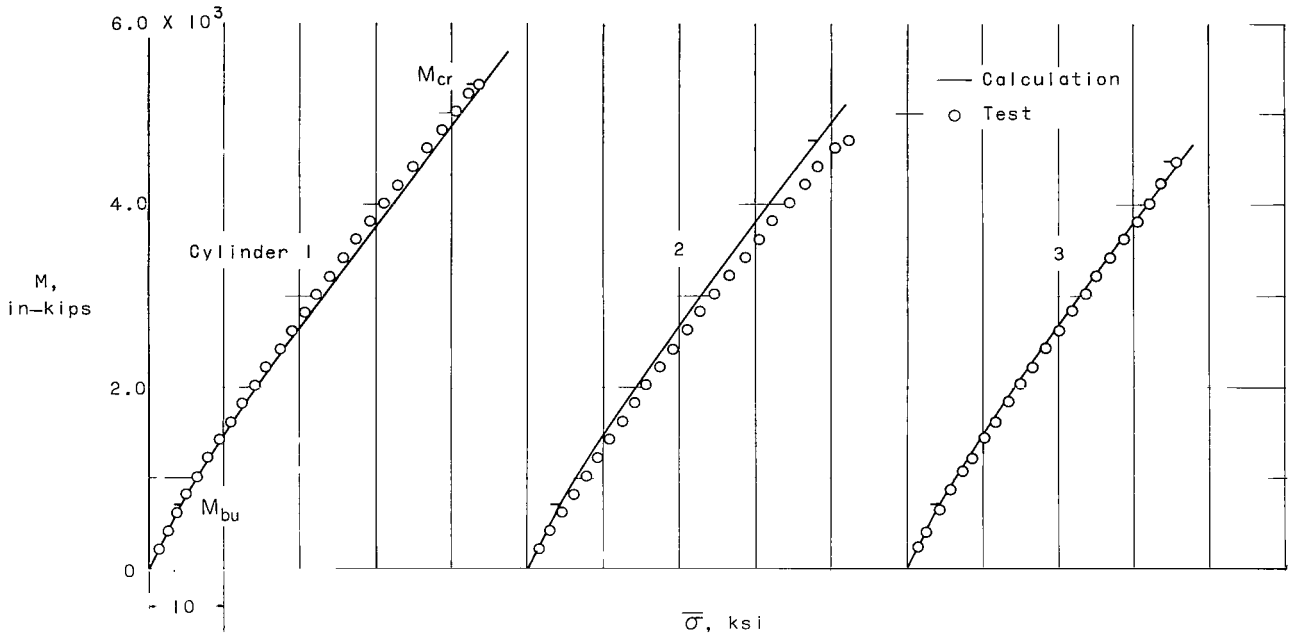


(a) Group I.

Figure 6.- Maximum stress in test cylinders due to applied load.

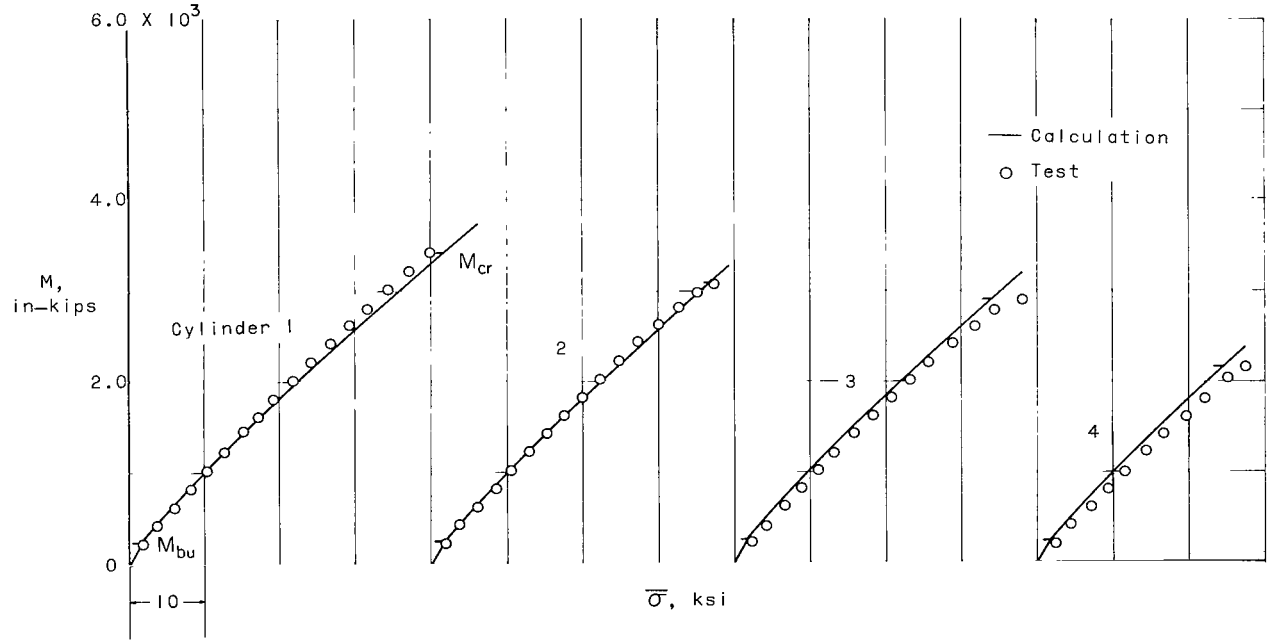


(b) Group II.

Figure 6.- Concluded.

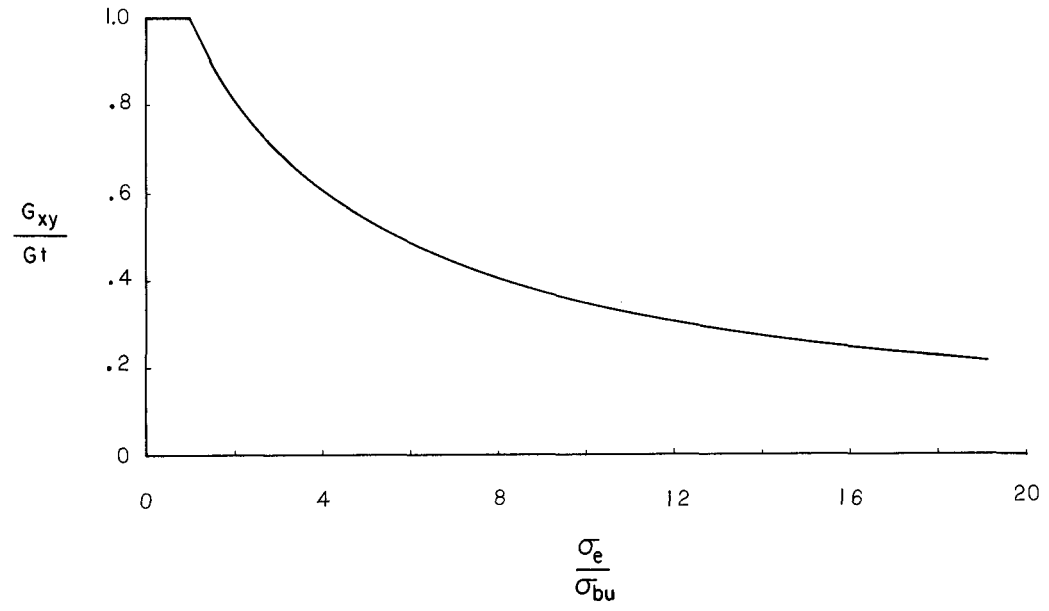


Figure 7.- Effective shearing stiffness of a buckled flat strip. (Data obtained from ref. 8.)

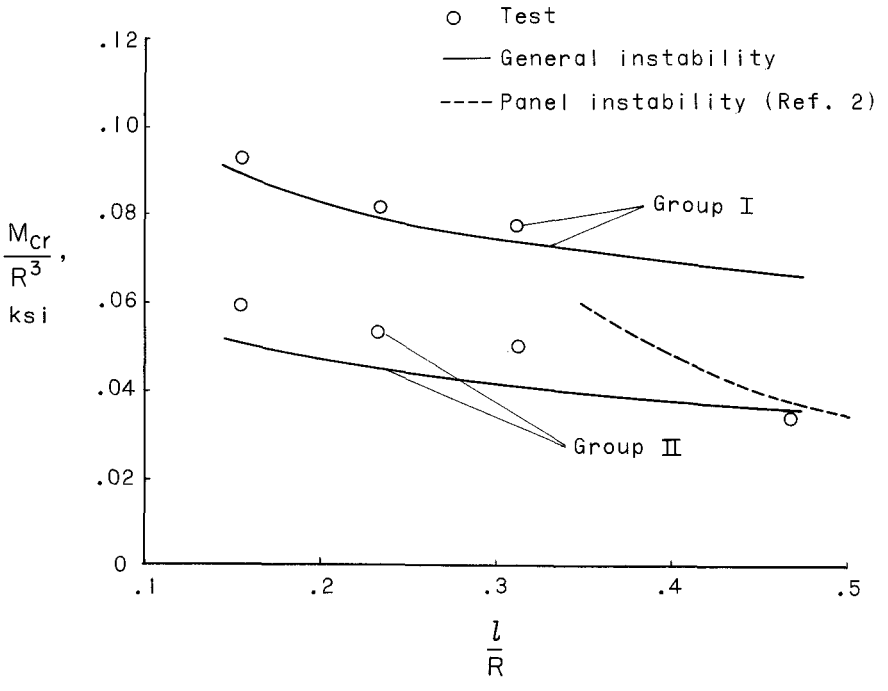


Figure 8.- Comparison of analysis and experiment for general and panel instability buckling of test cylinders.

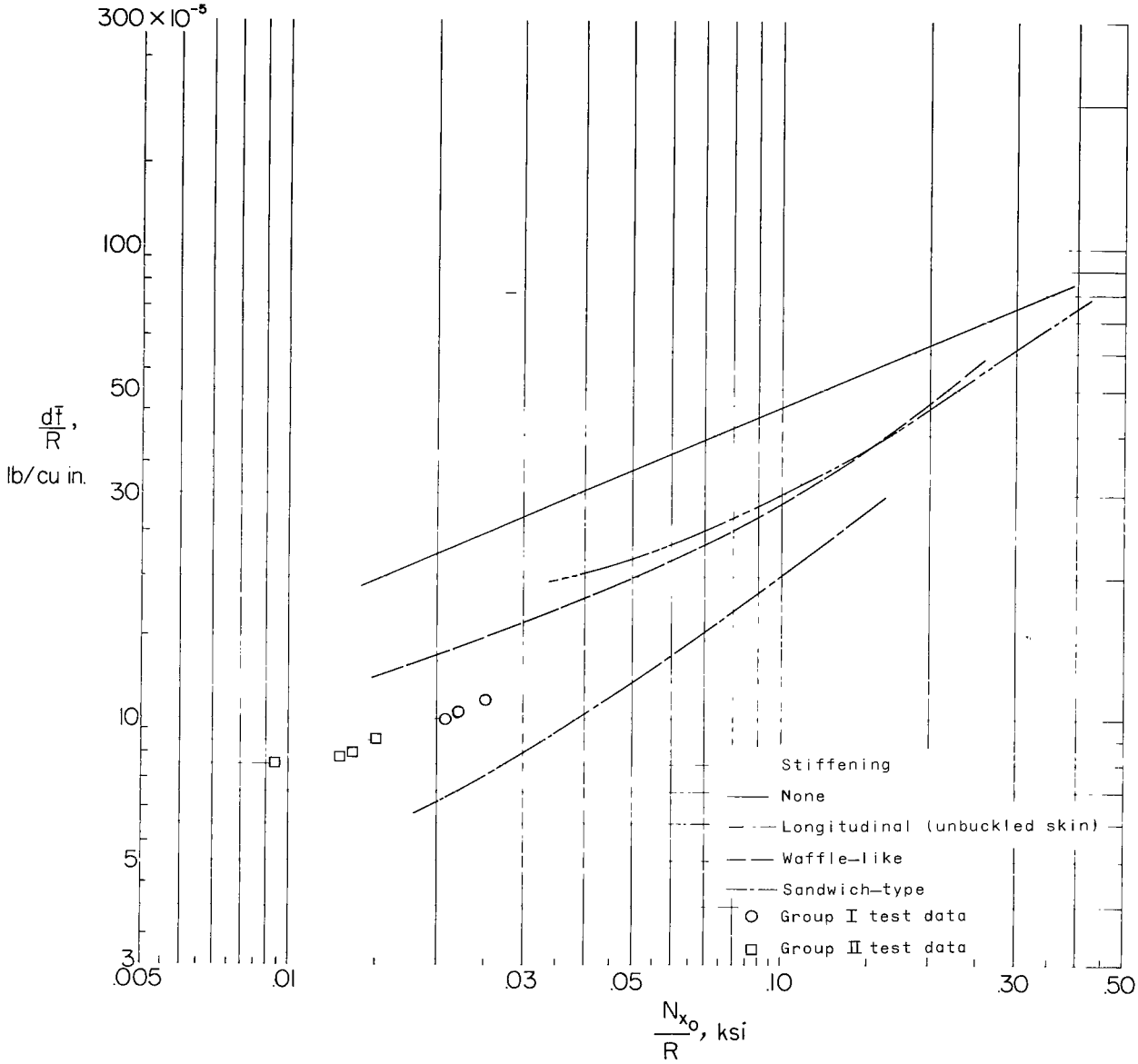


Figure 9.- Relative structural efficiency of test cylinders.

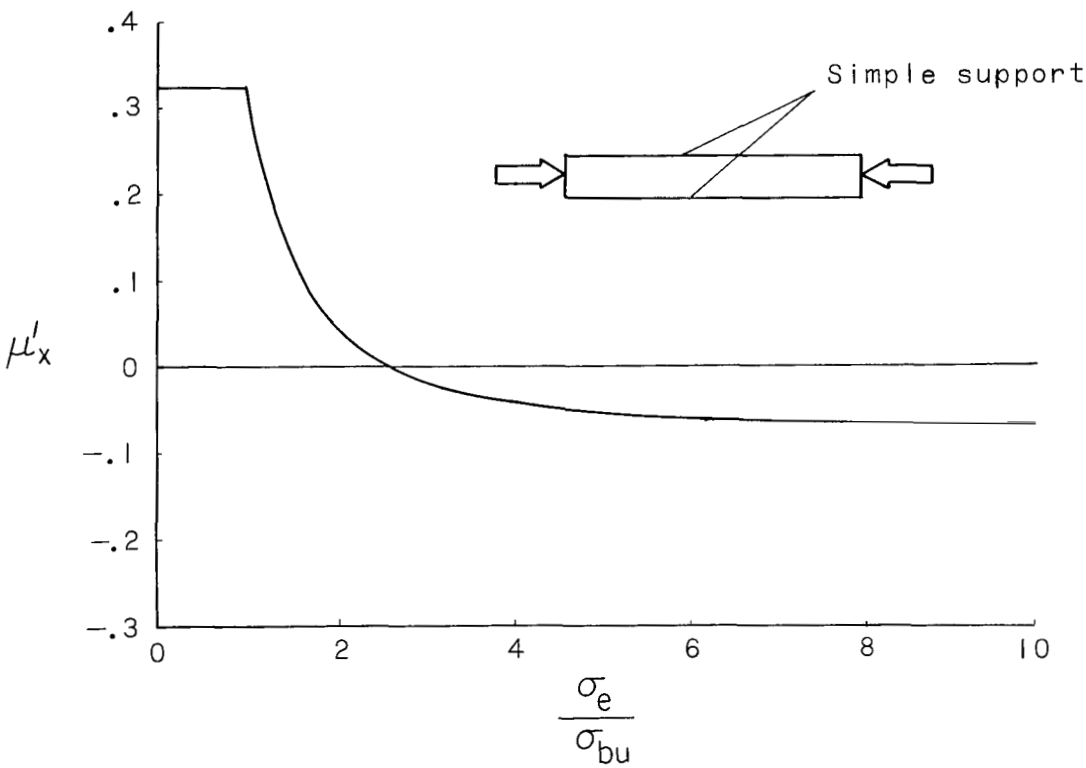


Figure 10.- Apparent value of Poisson's ratio for buckled, infinitely long, flat plate. (Data obtained from ref. 9.)

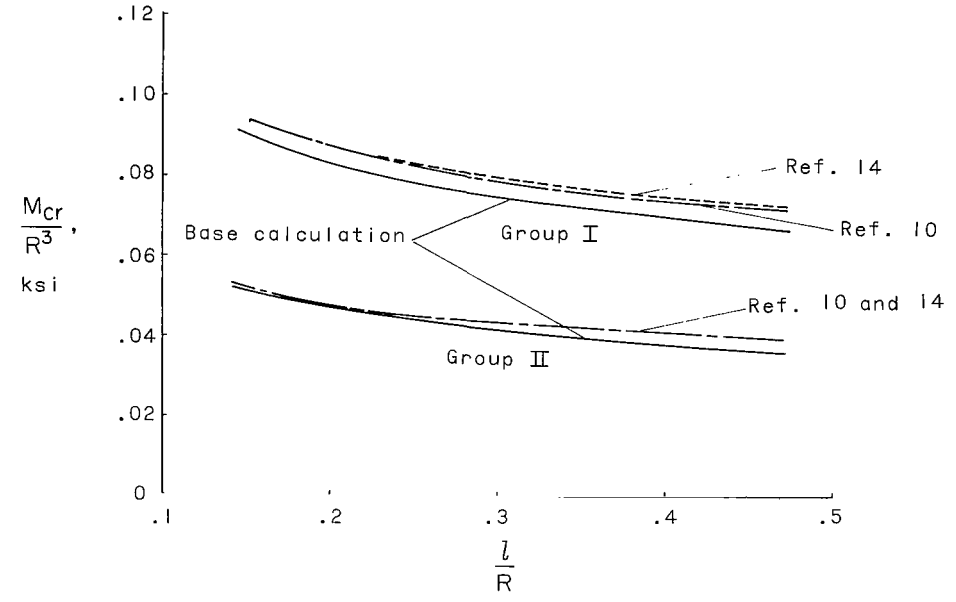


(a) Variations in $E_y$ and $D_y$.

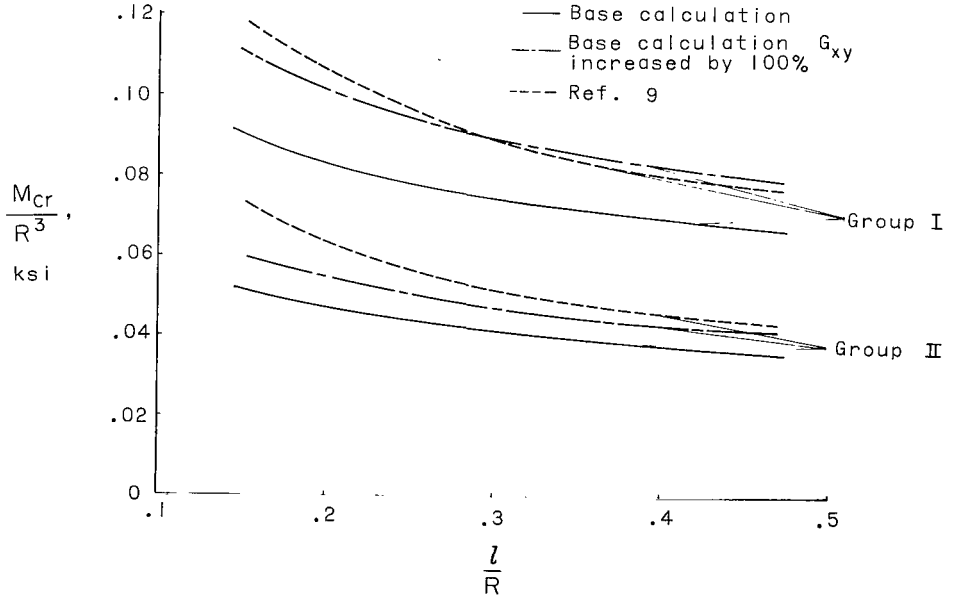


(b) Variations in $G_{xy}$.

Figure 11.- Effect of stiffness variations on the predicted general instability buckling loads for test cylinders.

2 17 R2

*"The National Aeronautics and Space Administration . . . shall . . . provide for the widest practical appropriate dissemination of information concerning its activities and the results thereof . . . objectives being the expansion of human knowledge of phenomena in the atmosphere and space."*

—National Aeronautics and Space Act of 1958

# NASA SCIENTIFIC AND TECHNICAL PUBLICATIONS

TECHNICAL REPORTS: Scientific and technical information considered important, complete, and a lasting contribution to existing knowledge.

TECHNICAL NOTES: Information less broad in scope but nevertheless of importance as a contribution to existing knowledge.

TECHNICAL MEMORANDUMS: Information receiving limited distribution because of preliminary data, security classification, or other reasons.

CONTRACTOR REPORTS: Technical information generated in connection with a NASA contract or grant and released under NASA auspices.

TECHNICAL TRANSLATIONS: Information published in a foreign language considered to merit NASA distribution in English.

TECHNICAL REPRINTS: Information derived from NASA activities and initially published in the form of journal articles or meeting papers.

SPECIAL PUBLICATIONS: Information derived from or of value to NASA activities but not necessarily reporting the results of individual NASA-programmed scientific efforts. Publications include conference proceedings, monographs, data compilations, handbooks, sourcebooks, and special bibliographies.

*Details on the availability of these publications may be obtained from:*

SCIENTIFIC AND TECHNICAL INFORMATION DIVISION

NATIONAL AERONAUTICS AND SPACE ADMINISTRATION

Washington, D.C. 20546